The Astronomical Journal, 138:1520–1528, 2009 November doi:10.1088/0004-6256/138/5/1520

TIME VARIABILITY IN THE OUTER EDGE OF SATURN'S A-RING REVEALED BY CASSINI IMAGING

J. N. Spitale and C. C. Porco
CICLOPS, Space Science Institute, 4750 Walnut St., Ste 20, Boulder, CO 80301, USA; joes@ciclops.org
Received 2009 May 29; accepted 2009 September 8; published 2009 October 15

ABSTRACT

We examine the outer edge of Saturn's A-ring, whose shape is strongly influenced by the co-orbital satellites Janus and Epimetheus, during the period from day 2005-121 to day 2009-036. Twenty-four Cassini imaging data sets are used, each one giving a picture of the ring during a short interval, allowing us to explore its time variability in detail for the first time. We find that the ring experienced a period of adjustment within ∼8 months of the 2006 January co-orbital swap, corresponding to the interval during which the two satellites were within about 60° of one another. Outside that adjustment period, the ring is dominated by an $m = 7$ pattern, as expected near a 7:6 inner Lindblad resonance, but the alignment is opposite in phase to that predicted for isolated test particles, and the amplitude of the radial distortion varies with time. We find that the amplitude variation corresponds to a beat pattern between the perturbations from the two satellites as would be expected if the responses add linearly. However, we also find deviations of limited azimuthal extent from the simple $m = 7$ pattern. Some of the additional structure may arise from coupling between the two excited modes in the ring, but the origin of these features is still under investigation.

Key words: planets: rings

1. INTRODUCTION

It has long been known that the outer edge of the A-ring is anchored and sculpted by the 7:6 inner Lindblad resonance with the co-orbiting satellites Janus and Epimetheus (Porco et al. 1984). Such a resonance should impose a seven-lobed distortion on the particle streamlines comprising the ring edge. However, the problem is complicated at the A-ring outer edge by the presence of two closely spaced satellites, as well as by the fact that the satellites experience abrupt semimajor axis changes at four-year intervals. The co-orbitals are in a 1:1 corotation resonance, with each satellite executing horseshoe motion in a frame rotating with the satellites' mass-weighted average mean motion (Yoder et al. 1983). In the inertial frame, the satellites swap orbits every 4.00 years with one moving slightly inward and one moving slightly outward.

Using *Voyager* imaging and occultation data, Porco et al. (1984) reported a seven-lobed pattern rotating at the mass-weighted mean angular speed of the co-orbital system with an amplitude of 6.7 km ± 1.5 km. However, that study was based on only 10 observations spanning the nine-month separation between the *Voyager 1* and *2* encounters with Saturn. Here, we re-examine the outer edge of the A-ring using thousands of high-resolution (1–10 km pixel-scale) images taken by the Narrow-Angle Camera (NAC) of the Cassini Imaging Science Subsystem (ISS; Porco et al. 2004) spanning nearly four years. With these data sets, we are able to observe a nearly complete azimuthal picture of the ring edge at each of numerous epochs, allowing us to characterize its variation in time.

2. RING KINEMATIC MODELS

To model the kinematics of ringlets and ring edges at a particular epoch, we attempt to identify the normal modes excited in the ring. Nearby shepherding satellites can be responsible for the confinement of narrow rings as well as the excitement of low-wavenumber normal modes (Goldreich & Tremaine 1982; Porco & Goldreich 1987) (They can also produce high-wavenumber waves in the edges of rings, as Pan and Daphnis do to their respective gap edges; Porco et al. 2005). Resonant interactions with distant satellites can do the same (Goldreich & Tremaine 1982). The most important such resonance in Saturn's rings is the inner Lindblad resonance produced by a satellite orbiting exterior to the rings. A particle's epicyclic frequency κ, which gives its radial variation, differs from its angular mean motion n by an amount equal to its apsidal precession rate $\dot{\varpi}$, whose nonzero value is a response to the oblateness of the planet:

$$\kappa = n - \dot{\varpi}. \tag{1}$$

For a nearly circular ring, a Lindblad resonance occurs where a test particle's epicyclic frequency is commensurate with a component of the orbital frequency of a perturbing satellite. In other words, $\kappa = \pm m(n - \Omega_p)$, where m is an integer and the pattern speed Ω_p is the angular speed of the mth Fourier component of the perturbing satellite's potential, given by

$$m\Omega_p = mn' + k\kappa', \tag{2}$$

where m and k are integers, and the primes denote satellite quantities (the vertical part of the perturbation is neglected here). Therefore the condition for a Lindblad resonance is

$$(m \mp 1)n \pm \dot{\varpi} - m\Omega_p = 0, \tag{3}$$

where the upper sign refers to the inner resonance. Using the definition of the pattern speed (Equation (2)), we have for the inner Lindblad resonance

$$(m + k)n' - (m - 1)n - k\dot{\varpi}' - \dot{\varpi} = 0. \tag{4}$$

Because precession rates are slow compared to mean motions, it is customary to label inner Lindblad resonances simply as $m+k : m-1$. Moreover, the strongest resonances are those of first order, i.e., with $k = 0$, so we limit the remainder of this discussion to that case. Near such a resonance, the collection of all particles with a given semimajor axis a comprises a streamline whose planetocentric radius as a function of longitude θ and time t in the inertial frame has the form

$$r(\theta, t) = a\{1 - e\cos m[\theta - \varpi_0 - \Omega_p(t - t_0)]\}, \tag{5}$$

Table 1
Semimajor Axes and Mean Motions for Janus and Epimetheus Before and After the 2006 January Co-orbital Swap

Element	Janus[b]	Epimetheus[b]	Janus[c]	Epimetheus[c]
a (km)[a]	151460.	151410.	151441.	151489.
$n(^\circ\text{day}^{-1})$	518.2388834	518.4828200	518.3456496	518.0977851

Notes.
[a] Semimajor axis of the ellipse; independent of n (a and n cannot always be linked by a simple relation because the orbit fits often do not consider every perturbation).
[b] For the period between 2002 January and 2006 January (Spitale et al. 2006).
[c] For the period between 2006 January and 2010 January (R. A. Jacobson 2009, private communication).

where e is the eccentricity and ϖ_0 is the periapse longitude at time t_0 (Goldreich & Tremaine 1982). Note from the definition of Ω_p (Equation (2)) that the pattern speed for a first-order Lindblad resonance is equal to the perturber's mean motion. Moreover, the perturber will stay aligned with either one apoapse or one periapse of the pattern, depending on whether the streamline is exterior or interior to the resonant location, respectively (Goldreich & Tremaine 1982).

Depending on the dynamical circumstances, a ring may exhibit contributions from multiple normal modes moving with various pattern speeds, in which case Equation (5) will include terms describing those additional modes, i.e.,

$$r(\theta, t) = a\left\{1 - \sum_{i=0}^{n} e_i \cos m_i\left[\theta - \varpi_0^{(i)} - \Omega_p^{(i)}(t - t_0)\right]\right\}. \quad (6)$$

This assumption of linear superposition is not automatically justified, however, and the true ring response may reflect an interaction between the constituent modes, which will appear as deviations from the shape predicted by Equation (6).

3. JANUS AND EPIMETHEUS

The A-ring edge is located near the 7:6 inner Lindblad resonances with the co-orbital satellites Janus and Epimetheus (Porco et al. 1984). These satellites are in a 1:1 corotation resonance with one another, each satellite executing horseshoe motion in the rotating frame (Yoder et al. 1983). In the inertial frame, the satellites appear to "swap" orbits every 4.00 years with Janus moving inward/outward by about 20 km, and Epimetheus moving outward/inward by about 80 km in semimajor axis. Because the satellites' orbits are not identical, the individual resonances have different radial locations. Moreover, the resonances change position whenever the satellites swap orbits.

Most of the images used in this study were obtained between the 2006 January and 2010 January co-orbital swaps, during which time the larger satellite, Janus, was interior. Elements for the current and previous configurations are given in Table 1. To get an idea of the relative contributions from each resonance to the total response, we can compare the radial amplitudes forced by each satellite. An isolated particle with semimajor axis a, a distance Δa from a first-order Lindblad resonance at a_0, undergoes radial oscillations of amplitude (Goldreich & Tremaine 1982)

$$ae_f = \frac{A}{\Delta a}, \quad (7)$$

where e_f is the forced eccentricity, and A is given by

$$A = \frac{M'}{M}\frac{\alpha a^2}{3(m-1)}\left(2m + \alpha\frac{d}{d\alpha}\right) b_{1/2}^{(m)}(\alpha)\Big|_{a_0}. \quad (8)$$

The masses of the satellite and planet are M' and M, $\alpha = a/a'$, and $b_{1/2}^{(m)}(\alpha)$ is a Laplace coefficient. Evaluating α at $a = a_0$, we have

$$\alpha_0 = \frac{a_0}{a'} = \left(\frac{n'}{n_0}\right)^{\frac{2}{3}} = n'^{\frac{2}{3}}\left(\frac{m-1}{mn' - \dot{\varpi}_0}\right)^{\frac{2}{3}}, \quad (9)$$

where n_0 and ω_0 are the mean motion and apsidal precession rate for a body with semimajor axis a_0, and Equation (3) has been used to rewrite n_0 in terms of n'. The co-orbitals' mean motions are much faster than the apsidal precession rate at the outer edge of the A-ring, so

$$\alpha_0 \simeq \left(\frac{m-1}{m}\right)^{\frac{2}{3}}, \quad (10)$$

for either satellite. Since α_0 has the same value for either satellite, the quantity A/M' is the same for both satellites, so the two Lindblad resonances induce forced eccentricities in the ratio

$$\frac{e_J}{e_E} = \frac{M'_J}{M'_E}\frac{\Delta a_E}{\Delta a_J}. \quad (11)$$

Between the 2006 and 2010 co-orbital swaps, the resonances for Janus and Epimetheus are located at 136,766 and 136,809 km, respectively. The mass of Janus is ~3.6 times that of Epimetheus (Spitale et al. 2006), so at the nominal ring edge with a = 136,773 km (Porco et al. 1984), Janus would be expected to induce a forced eccentricity in a test particle orbit nearly 2 orders of magnitude stronger than that from Epimetheus. Moreover, since the Janus resonance falls inside the ring, forced eccentricities from that resonance should be much larger still, limited only by inter-particle interactions. Therefore, we would expect the kinematics at the present time to be dominated by the resonance with Janus, which should produce a seven-lobed pattern co-rotating with that satellite.

4. DATA SETS

In this study, we used 24 data sets spanning the interval from day 2005-121 to day 2009-036, consisting of a total of more than 3300 Cassini NAC images (see Table 2), with pixel scales about 10 km pixel^{-1} or better. Images were discarded for several reasons including dropped lines, excessive blur, and poor signal to noise. The data sets comprise two broad types of observations—azimuthal scans and ansa staring movies. In an azimuthal scan, the camera is scanned around the ring, yielding broad azimuthal coverage. Azimuthal scans are well suited to studying ring shapes because they capture a nearly complete azimuthal picture of the ring during a short time interval (a full A-ring scan typically takes ~ 8 hr; the orbital period at the A-ring outer edge is ~ 15 hr). Unfortunately, azimuthal scans are difficult to obtain and require fairly specific geometry to maximize the unobscured extent of the ring, and therefore they are rare. Ansa movies, on the other hand, are relatively easy to obtain because the camera simply remains pointed at one ring ansa for the entire observation, generally an orbital period, while the ring material moves through the field of view. The apsidal

Table 2
Data Sets Used in this Study

Set No.	Date	Observation ID
2	2005-121	ISS_007RI_LPHRLFMOV001_PRIME[a]
3	2005-122	ISS_007RI_AZSCNLOPH001_PRIME[b]
4	2005-138	ISS_008RI_LPHRLFMOV001_PRIME[a]
14	2005-233	ISS_013RI_AZSCNHIPH002_PRIME[b]
20	2006-268	ISS_029RI_AZSCNLOPH001_PRIME[b]
22	2006-272	ISS_029RF_FMOVIE001_VIMS[a]
120	2007-058	ISS_039RF_FMOVIE001_VIMS[a]
121	2007-076	ISS_041RF_FMOVIE002_VIMS[a]
123	2007-090	ISS_041RF_FMOVIE001_VIMS[a]
48	2007-115	ISS_043RI_AZSCAN001_PRIME[b]
51	2007-335	ISS_053RI_LPHRDFMOV001_PRIME[a]
53	2007-365	ISS_055RF_FMOVIE001_VIMS[a]
55	2008-007	ISS_055RI_LPMRDFMOV001_PRIME[a]
57	2008-024	ISS_057RF_FMOVIE001_VIMS[a]
59	2008-075	ISS_061RI_LPMRDFMOV001_PRIME[a]
65	2008-113	ISS_065RI_LPHRLFMOV001_PRIME[a]
61	2008-137	ISS_068RF_FMOVIE001_VIMS[a]
62	2008-152	ISS_070OT_PAZSCN002_PRIME[b]
66	2008-216	ISS_079RF_FRINGMRDF002_PRIME[a]
135	2008-274	ISS_087RF_FMOVIE003_PRIME[a]
136	2008-289	ISS_089RF_FMOVIE003_PRIME[a]
138	2008-312	ISS_092RF_FMOVIE003_PRIME[a]
139	2008-319	ISS_093RF_FMOVIE003_PRIME[a]
142	2009-038	ISS_102RI_RETARMRLP002_PRIME[b]

Notes.
[a] Ansa movie.
[b] Azimuthal scan.

precession induced by Saturn's oblateness is $\sim 3^\circ$ day^{-1} in the outer A-ring, so the apsidal line rotates little during the time a movie is obtained. Consequently, any wavenumber $m = 1$ (i.e., precessing Keplerian ellipse) shape of the ring is poorly sampled in such a movie. However, because the resonant patterns with $m > 1$ rotate much faster in Saturn's rings than the apsidal precession rate, one or more full cycles of such a pattern can be captured during an ansa movie spanning a single orbital period. Each data set of each type provides a picture of the A-ring edge at that epoch, so we can examine the time variability of the pattern's shape and kinematics by treating each data set separately.

5. DATA REDUCTION

Although the Cassini imaging arrays are highly photometrically linear (Porco et al. 2004), we performed a radiometric calibration on each image in order to obtain the most photometrically linear possible representation of the image scene. Except near the corners, Cassini NAC images are geometrically accurate to better than 0.25 pixel (Porco et al. 2004), so we did not correct the images geometrically, though we avoided measuring features near the corners of images.

The camera orientation may be determined absolutely by registering the observed image locations of catalog stars with their known sky-plane locations. However, many of the images used in this study contain little sky and hence few stars on which to navigate, so we instead used known circular ring features and assigned these features the absolute radii determined from *Voyager* and 28 Sgr occultation data (French et al. 1993).

After the pointing was corrected, we extracted narrow scans or profiles of brightness versus radius from each image. The brightness at each point in the profile was computed by averaging across a 5-pixel-wide band at constant radius. For this work we extracted a single radial profile per image because this procedure produces a set of measurements for each ring edge that is small enough to manage efficiently, but still large enough (typically hundreds of profiles for a given data set) to provide an extremely detailed view of the ring shape at that epoch. This procedure typically provides an azimuthal spacing of $\sim 1^\circ$, so modes up to $m \sim 180$ could, in principle, be distinguished in each data set before we would need to increase the density of our measurements.

In order to remove any systematic effects in the navigation of each data set, we used the known radii of circular features derived from the work of French et al. (1993) to place all of our raw radius measurements on their radial scale, as in Porco et al. (1984). The result is a radial position "scaled" relative to the absolute position of the fiducial features.

The only French et al. (1993) fiducial feature available in every data set used in this work was the outer edge of the Keeler gap (feature number 1 in French et al. 1993). However, we now know that near the longitude of the recently discovered satellite Daphnis (Porco 2005) the outer edge of the Keeler gap is perturbed, with an amplitude of about 2 km, so we did not use observations taken within 5° of Daphnis' longitude. Even so, we see some "noise" in the registration in some places at the 1–2 km level. However, as seen in Section 6, when discussing structure at that level, we were careful to examine the Keeler gap edge for variations that could produce such false structure on the A-ring edge.

Because there was only a single fiducial available, we were able only to correct the radial offset for each data set, with no correction to the scaling factor (i.e, km pixel^{-1}). However, the relative proximity of our fiducial to our feature of interest mitigates the fact that we must rely on the assumed ephemeris (from SPICE files Acton 1990) for the radial scaling: with typical spacecraft-to-ring ranges of $\sim 15 R_s$, and a worst-case ephemeris uncertainty of $\sim$ 10 km (1–2 km is typical; Antreasian et al. 2006), the relative error in the radial scaling is about 10^{-5}, yielding an insignificant radial error of about 2.5 m over the 250 km distance from the Keeler gap edge to the A-ring edge.

Determination of the radial location of a sharp ring edge is complicated by the dispersion of light in the camera optics, which is characterized by a point-spread function (PSF). To estimate the radius corresponding to the actual ring edge, we followed the procedure of Porco et al. (1984), measuring the radius at which the brightness profile attained a value halfway between the maximum and minimum values in a window surrounding the edge. The uncertainty in the measurement of each feature radius was taken to be proportional to the observed width of the edge in each measured profile. That width was measured by finding the inflection points on each side of the transition. Based on our experience with the Cassini imaging data sets, we took 0.1 as the constant of proportionality between the measured feature width and the adopted uncertainty in the radial location of the edge. We also accounted for the 0.7 km uncertainty in the fiducial radii given in French et al. (1993).

The longitude uncertainty was neglected. At the ansa, a pixel may span 50 km (though 20 km or less is typical) in the azimuthal direction, but that is still only $0.^\circ 02$ in longitude, and the image registration in the azimuthal direction is typically better than a pixel because the projected ring has its greatest curvature on the ansa. Near quadrature, the azimuthal registration is less precise, but the pixel scale in the azimuthal direction is much finer. A typical azimuthal pixel scale in this geometry would

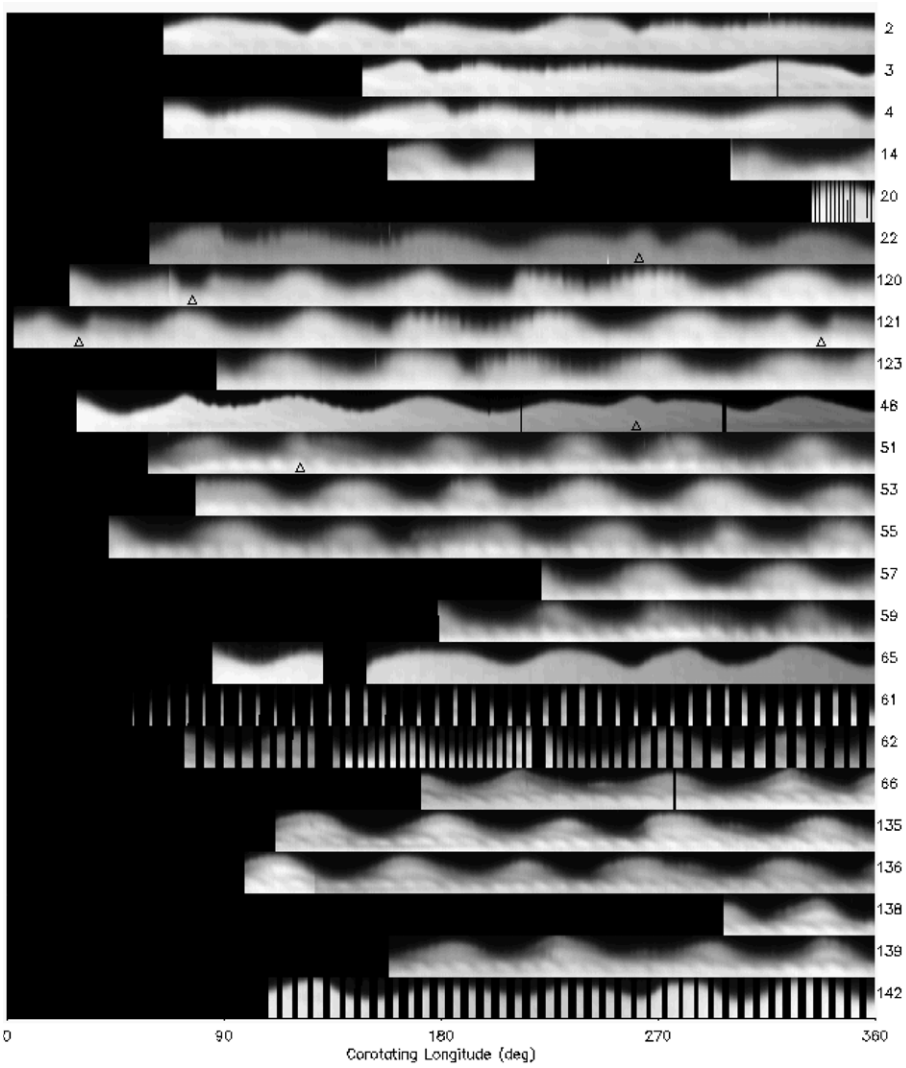

Figure 1. Mosaics in radius vs. longitude for the Cassini data sets used in this study. The first image in each data set is assigned a longitude of zero. Later images are mapped successively to the left (i.e., decreasing in longitude from 360°) according to their inertial longitudes, corrected for pattern rotation at Janus' present mean motion. Particles at the ring edge move through the mosaic from left to right. For each mosaic, radii range from 136,715 to 136800 km. The expected seven lobes are visible in most data sets, but there is additional structure, including short-wavelength undulations, as well as anomalous broad radial features, which are indicated by triangles. Note that the same feature is mapped twice in set 121.

be, say, 5 km; a rather large 10-pixel registration error would again give a 0.°02 longitude error. In either case, the longitude error is typically smaller than the $m = 7$ wavelength by a factor of more than 10^3; by comparison, radial uncertainties are more like 1/10 of the peak-to-peak radial amplitude of the ring.

A nonlinear least-square gradient-expansion algorithm (Press 1992) was used to determine best-fit streamline elements for a model consisting of the superposition of a variable number of normal modes as in Equation (6). Periapse longitudes $\varpi_0^{(i)}$ for each normal mode are precessed to a common epoch using an assumed or fit pattern speed $\Omega_p^{(i)}$. For each measurement, residuals are computed between that precessed model and the measured radius at the measured longitude. The solution is determined by searching down the χ^2 gradient until a sufficiently small change in χ^2 is obtained.

6. RESULTS

Figure 1 shows mosaics in radius versus longitude for the Cassini data sets used in this study. The large-amplitude periodicity apparent in most of the data sets shows the expected seven lobes, though the shape deviates significantly from a sinusoid. Although most of the power appears to be in the expected $m = 7$ normal mode precessing at a rate close to that of Janus, we searched for solutions with wave numbers $m = 6$ and $m = 8$ and found none that were satisfactory, even with the pattern speed free. In addition to the expected seven lobes, the figure shows short-wavelength undulations spanning about 90° of longitude in some scans, as well as other anomalous radial perturbations, some appearing as radial incursions into the ring, and others appearing as radial excursions, as if an extra lobe were dropped into the background $m = 7$ pattern (indicated by triangles in the figure).

6.1. $m = 7$ *Pattern*

Figure 2 shows fits to an $m = 7$ normal mode with a, e, and ϖ_0 free, for every data set. For these fits, the pattern speed Ω_p was fixed at Janus' mean motion, for the reasons given in Section 3. Because some of the more prominent radial anomalies resemble lobes of the $m = 7$ pattern, they were removed before performing the fits. For each data set, the fit is well behaved with respect to a and e; that is, there is only one χ^2 minimum in those dimensions. Solutions for ϖ_0 are not unique, but the

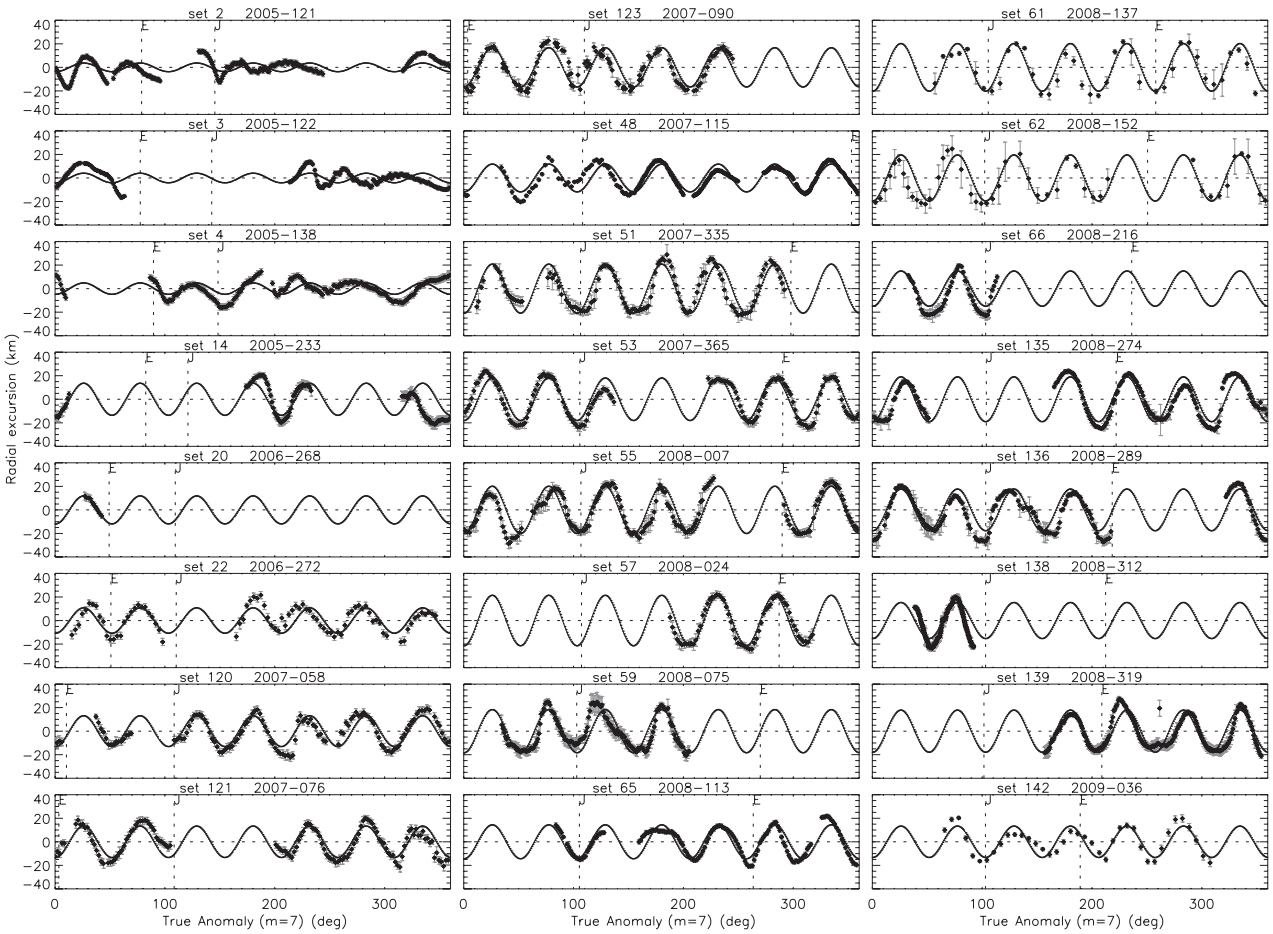

Figure 2. True anomaly vs. radius for an $m = 7$ pattern moving at Janus' mean motion, for each data set used in this study. The solid curve shows the best-fit pattern (with a, e, and ϖ free); dashed vertical lines indicate the positions of Janus (J) and Epimetheus (E) at each epoch. Data set numbers and observation dates are given above each graph. For data sets obtained within about eight months of the 2006 January co-orbital swap, the pattern is scrambled; also the apsidal alignment with Janus is not evident until nearly a year after the swap.

seven possible outcomes are degenerate. Table 3 gives the fit elements for each imaging data set at the J2000 epoch. The $m = 7$ pattern dominates the kinematics, but the ring edge is clearly more complicated, as reflected by the relatively large fit residuals and χ^2 values. The fit semimajor axes, a, vary from 136,758 km to 136,778 km, probably as a result of incomplete or sparse sampling of the complicated shape. The fit amplitudes, ae, vary from less than 5 km to greater than 20 km.

The apsidal alignment is opposite to that predicted by the theory for an isolated particle near a Lindblad resonance. Streamlines exterior to the resonance, like those at the A-ring edge, should have one apoapse oriented toward the satellite; instead, we observe one periapse to track Janus. This configuration is also seen at the outer edge of the B ring (Porco et al. 1984) and suggests that ring material external to the resonance has its phase locked with the help of material internal to the resonance, a consequence of inter-particle interactions (Borderies et al. 1982; Porco et al. 1984).

Inspection of Figure 2 reveals an interesting trend: the radial variations in the earlier data sets are less regular than in the later data sets. The early data sets (2, 3, 4, 14), which were obtained before the 2006 January co-orbital swap (about 5 to 9 months prior), show a large-amplitude quasi-periodic variation, but the individual lobes are phased irregularly, resulting in a poor fit to the pure normal mode. The three smallest eccentricities in Table 3 are associated with those poor pre-swap fits. The data sets obtained after the swap (the first of which was obtained about eight months after the swap) show some short-period amplitude variation, but the shape is a better fit to the pure $m = 7$ pattern. We interpret these trends to reflect a period of adjustment during which the ring edge was responding to the configuration change. That interpretation is consistent with the observation that the apsidal alignment with Janus was not established until nearly a year after the swap, as is evident in Figure 2.

To obtain an average pattern speed, we fit all of the post-swap imaging data sets (i.e., those obtained on or after 2008-268, after the ring had settled into its present configuration) simultaneously to the $m = 7$ model with the pattern speed as an additional free parameter. Figure 3 shows the resulting model; the elements at the J2000 epoch, with formal 1σ uncertainties, are as follows (the uncertainties are given in parentheses and refer to the least significant digit):

$$\begin{aligned} a &= 136,768.9(3)\ \text{km} \\ e &= 10.5(3) \times 10^{-5} \\ \varpi_0 &= 46.2(2)^\circ \\ \Omega_p &= 518.354(1)^\circ\ \text{day}^{-1} \\ \chi^2/\text{DOF} &= 12.2 \\ \text{RMS} &= 8.6\ \text{km}. \end{aligned}$$

The pattern speed differs from Janus' mean motion by $0\overset{\circ}{.}007\ \text{day}^{-1}$, the equivalent of several σ. Fixing the pat-

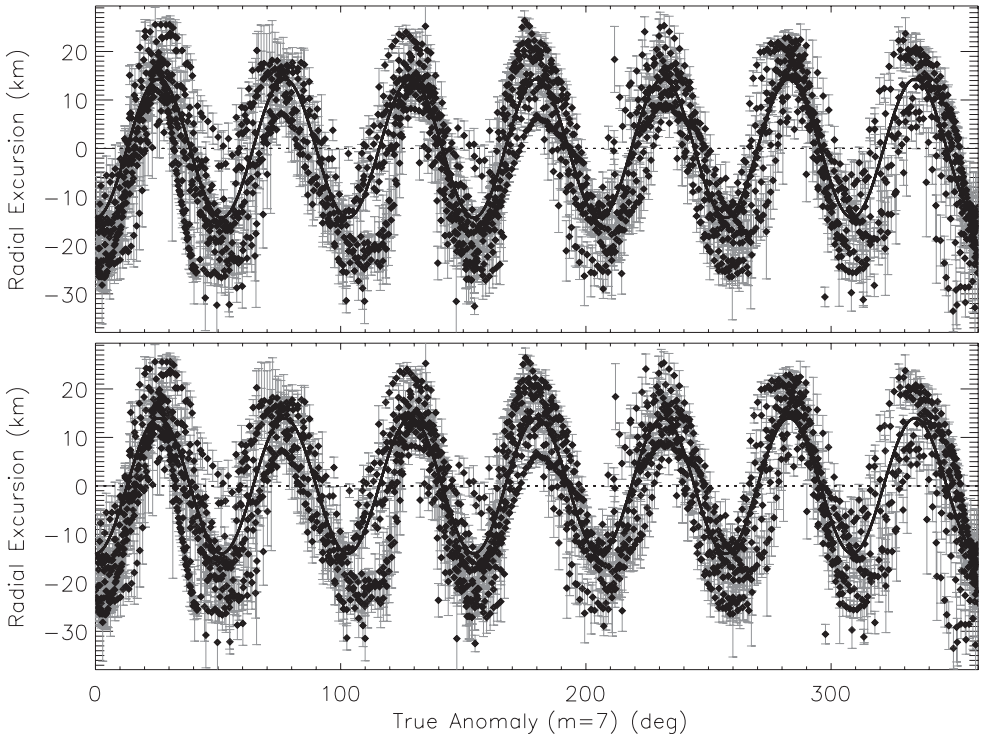

Figure 3. Simultaneous fits to all data sets in this study occurring on or after day 2006-268. In both plots, a, e, and ϖ were allowed to vary. In the top plot, the pattern speed Ω_p was also varied, so as to determine its mean value. In the bottom plot, the pattern speed was fixed at Janus' mean motion. The fits are nearly indistinguishable, consistent with the observation that the pattern is aligned with Janus.

Table 3
Best-Fit Streamline Elements with Formal 1σ Errors for the A-ring's $m = 7$ Mode Moving at Janus' Mean Rate

Set	a (km)	$e \times 10^{-5}$	$\varpi_0(^\circ)$[a]	RMS (km)	χ^2/DOF
2	136776.9(5)	2.7(5)	10.(1)	6.4	13.5
3	136772.1(5)	3.0(5)	13.(1)	6.6	22.3
4	136774.1(5)	3.5(5)	4.(1)	6.4	6.6
14	136768.(1)	10.(1)	22.9(8)	11.5	12.0
20	136776.3(6)	8.7(2)	17.2(5)	0.4	0.03
22	136767.6(7)	7.9(8)	15.8(7)	6.8	5.6
120	136772.1(5)	9.6(6)	18.1(5)	6.0	4.2
121	136774.1(6)	9.8(6)	18.7(5)	6.1	3.6
123	136771.8(7)	12.2(6)	16.7(4)	6.8	3.6
48	136768.6(2)	8.6(2)	19.1(2)	4.4	17.5
51	136765.2(6)	15.2(6)	21.2(3)	7.7	3.5
53	136767.3(6)	13.2(6)	20.5(4)	7.0	6.1
55	136764.1(5)	14.7(6)	20.8(3)	8.0	4.8
57	136767.9(6)	15.7(6)	18.7(3)	5.4	2.4
59	136762.3(6)	13.4(6)	23.1(3)	7.4	2.4
65	136768.0(5)	10.5(5)	22.0(4)	5.4	12.5
61	136760.(2)	15.(2)	21.8(8)	8.5	10.4
62	136758.(1)	14.(1)	23.6(7)	8.4	3.1
66	136775.(1)	11.(1)	24.1(8)	8.0	12.2
135	136768.7(6)	13.9(6)	22.4(4)	7.9	20.8
136	136769.0(6)	12.9(6)	23.6(3)	8.1	12.3
138	136765.6(8)	11.2(8)	23.6(5)	9.1	18.8
139	136767.8(5)	13.1(5)	24.8(3)	7.0	7.0
142	136774.1(9)	9.8(9)	23.5(7)	5.8	10.5

Note. [a] At the J2000 epoch.

tern speed at Janus' mean motion, the following elements are obtained:

$$a = 136,769.0(3)\ \text{km}$$
$$e = 10.1(3) \times 10^{-5}$$
$$\varpi_0 = 20.7(2)^\circ$$
$$\Omega_p = 518.3456496^\circ\ \text{day}^{-1}$$
$$\chi^2/\text{DOF} = 13.5$$
$$\text{RMS} = 9.1\ \text{km}.$$

The formal statistics suggest that the difference between the two fits is significant, but the plots in Figure 3 show that the two models are nearly indistinguishable. The difference between the fits is most likely due to the fact that the co-orbitals' mean motions are not truly constant between swaps (Yoder et al. 1983). The fit semimajor axis is consistent with the value of 136,773 ± 8 km determined by Porco et al. (1984).

Table 3 reveals a significant eccentricity variation among our data sets. Even ignoring data sets taken close to the co-orbital swap (sets 2, 3, 4, 14), as well as data sets where only about one lobe or less is sampled (sets 20, 61, 66, 138), the eccentricity appears to vary with time. Figure 4 shows the amplitudes ae as a function of time for the remaining data sets. The curve is a sinusoidal fit to the amplitudes, excluding the obvious outliers – sets 123, 51, 62, and 139. The fit sinusoid has a period of 209 ± 1 days, precisely 1/7 the 1461-day synodic period of the two satellites. We interpret this as a beating between responses raised by the two satellites.

When the amplitudes of the two components are the same, the phenomenon of beating between signals with frequencies ω_1 and ω_2 can be understood using the well-known cosine addition formula

$$\psi_0(t) = \cos\omega_1 t + \cos\omega_2 t = 2\cos\left(\frac{\omega_1+\omega_2}{2}\right)t\cos\left(\frac{\omega_1-\omega_2}{2}\right)t. \quad (12)$$

The resulting signal is composed of a signal at the mean frequency, modulated by an envelope with frequency $\frac{1}{2}(\omega_1-\omega_2)$.

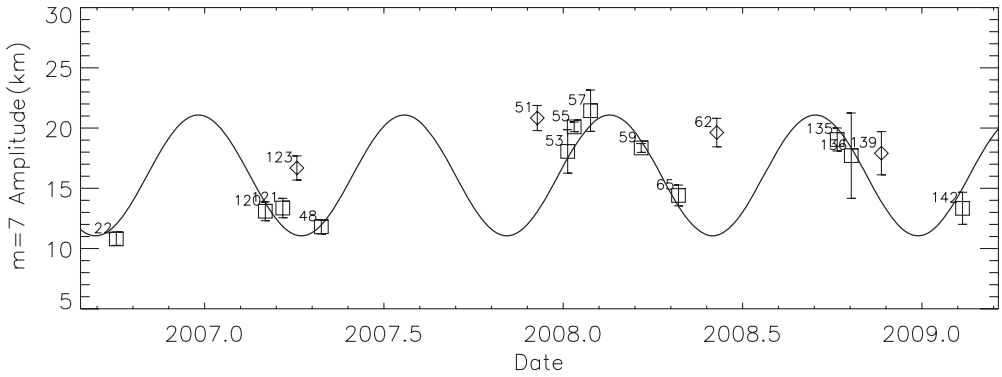

Figure 4. Radial amplitudes as a function of time for data sets obtained more than eight months after the 2006 January co-orbital swap. Data sets for which the azimuthal sampling was inadequate for determining a reliable amplitude were excluded. The solid curve shows a fit to the data points marked with square symbols, and has a period of 209 ± 1 days, consistent with a beating between the Janus and Epimetheus perturbations. Points marked with diamonds were omitted from the fit (see text).

However, in the case of Janus and Epimetheus, the signals have different amplitudes,

$$\psi(t) = A_1 \cos \omega_1 t + A_2 \cos \omega_2 t, \tag{13}$$

so Equation (12) does not accurately describe the net response. Defining,

$$\nu = \frac{\omega_1 - \omega_2}{2} \text{ and } \omega = \frac{A_1\omega_1 + A_2\omega_2}{A_1 + A_2} \equiv \frac{A_1\omega_1 + A_2\omega_2}{A}, \tag{14}$$

and using complex exponential notation,

$$\psi(t) = A_1 e^{i\omega_1 t} + A_2 e^{i\omega_2 t}, \tag{15}$$

$\psi(t)$ can be factored as

$$\psi(t) = e^{i\omega t}\left[A_1 e^{i\gamma_2 \nu t} + A_2 e^{-i\gamma_1 \nu t}\right], \tag{16}$$

where $\gamma_1 = 2A_1/A$ and $\gamma_2 = 2A_2/A$. Expression (16) is not as simple as it looks. Although the term in brackets is not in general periodic (the sum of two trigonometric functions is periodic only when the two frequencies are commensurate), each of its two components modulates the primary signal, whose frequency is ω, the amplitude-weighted mean frequency of the input signals. The phases of the two components conspire to modulate the net signal at frequency ν.

As in the simple case, the beat frequency ν depends only on the two input frequencies because the beating arises from the alternating periods of constructive and destructive interference between the patterns, independent of their respective amplitudes. For the same reason, the peak-to-peak amplitude of the beat envelope is simply $|A_1 - A_2|$. On the other hand, the primary frequency ω depends on the relative amplitudes of the two primary signals, approaching that of the dominant signal as its amplitude becomes large relative to the other. In the case of the A-ring edge at the present time, Janus' perturbations are much stronger than those from Epimetheus (see Section 3), so Janus' pattern speed dominates, as observed. However, the beating caused by Epimetheus' relatively tiny additional perturbation should not be distinguishable from the noise. The fact that an obvious beat pattern is observed suggests an enhancement by some interaction between the two modes, as in Longaretti (1989).

The observed beating between the two resonant responses motivates a search for a two-component model to fit all of the post-swap data sets, i.e,

$$r(\theta, t) = a\Big\{1 - e_E \cos 7\big[\theta - \varpi_0^{(E)} - \Omega_p^{(E)}(t - t_0)\big] - e_J \cos 7\big[\theta - \varpi_0^{(J)} - \Omega_p^{(J)}(t - t_0)\big]\Big\}, \tag{17}$$

where the E and J scripts indicate elements associated with the response to each satellite. Each component has wavenumber 7, and a pattern speed corresponding to the mean motion of the indicated satellite, as given in Table 1. The resulting best-fit J2000 elements are as follows:

$$\begin{aligned} a &= 136{,}768.3(3) \text{ km} \\ e_J &= 10.5(3) \times 10^{-5} \\ e_E &= 1.7(3) \times 10^{-5} \\ \varpi_0^{(J)} &= 21.6(3)^\circ \\ \varpi_0^{(E)} &= 50.(1)^\circ \\ \chi^2/\text{DOF} &= 13.0 \\ \text{RMS} &= 9.1 \text{ km}. \end{aligned}$$

Statistically, this fit is about as good as the one-component models above, and the elements for the Janus component are nearly the same as those in the one-component solutions. Therefore, since adding an Epimetheus component to the fit did not change the result significantly, we conclude that the data are not of sufficient resolution for this fit to yield meaningful information about that component.

6.2. Radial Anomalies

The anomalous radial excursions seen in some data sets are difficult to characterize, but two or more distinct features can be identified. The "bumps" in sets 22 and 48 appear morphologically similar to one another and possibly to that in set 51. The interval between sets 22 and 48 (∼ 7 months) is long enough to accommodate many possible pattern speeds, including ∼ 518° day^{-1} (close to Janus' rate) and ∼ 604° day^{-1} (close to the Keplerian rate at the A-ring edge), but the three sets together fit only the speed near the Keplerian rate. However, at either speed, the feature should have appeared in intervening data sets, but is not seen, though it may not be identifiable when it coincides with one of the $m = 7$ lobes. It is not clear whether we are looking at one, two, or three distinct features here, but Keplerian shear would destroy any such feature on a timescale shorter than the interval between any of these three data sets unless the features were being actively maintained.

The "dips" in sets 120 and 121 are almost certainly the same feature, as the data sets were obtained 18 days apart and the morphology is nearly identical (Note that the set 21 ansa movie lasted more than one Janus orbital period and therefore captured the same anomalous feature twice), with the later appearance apparently showing some Keplerian shear. If the pattern were moving at Janus' rate it would only appear once in the set-121 movie in Figure 1.[1] Moreover, the local Keplerian rate also fits the feature in set 120. Therefore this must be a single feature moving near the Keplerian rate at the A-ring outer edge.

Short-wavelength structure is evident in a number of data sets. The subtle jagged edge seen in sets 135, 136, and 139 (e.g., centered near 220° in set 135) is caused by registration errors propagated from the Keeler gap edge, but the more prominent undulations (e.g., centered near 140° in set 48) seen in data sets taken on or before day 2007-115—sets 2, 3, 22, 120, 121, 123, and 48—appear to be real. Specific features in the wavy pattern are difficult to track, but the motion is roughly consistent with the Keplerian rate at the outer A-ring edge. The fact that it appears stationary relative to the anomalous feature in sets 120 and 121 (count to the right the number of $m = 7$ troughs between the anomaly and the wavy pattern) corroborates this speed, though it would be difficult to distinguish a difference in speed of 1° day^{-1} or smaller.

The most obvious cause for a such wavy pattern is a nearby satellite. In the simplest treatment of a satellite perturbing a ring edge using the impulse approximation, a wavy pattern is created in the ring's edge with a wavelength given by $\lambda = 3\pi\Delta a$, where Δa is the satellite's distance from the edge. Pan and Daphnis both have such an effect on the edges of their respective gaps, Encke and Keeler, though in practice those patterns are quite complex (Weiss et al. 2009). For the pattern observed here, the wavelength appears to be consistent at $\lambda = 14300 \pm 1500$ km, or about 6° of longitude. According to this approximation, the satellite's semimajor axis should be $\Delta a = 14300 \pm 1500\,\mathrm{km}/3\pi = 1500 \pm 160$ km beyond the A-ring edge, well outside the orbit of Atlas ($\Delta a \simeq 900$ km) and well inside the orbit of Prometheus ($\Delta a \simeq 2600$ km; Spitale et al. 2006). Although the pattern is localized in azimuth, the 6° wavelength suggests a resonant perturbation with $m = 60$. However, the 60:59 Lindblad resonance would require a perturber in about the same position as that given by the impulse approximation because the mechanism for producing the pattern is essentially the same.

The impulse approximation can be used to relate the perturbing mass M' to the forced eccentricity e_f, given the radial offset Δa (Shu 1984):

$$\frac{M'}{M} = \frac{3}{4} e_f \left(\frac{\Delta a}{a}\right)^2, \tag{18}$$

where M is Saturn's mass. The pattern's amplitude ae_f is typically greater than 2 km, so the satellite would need a mass of $\sim 10^{18}$ kg, corresponding to a spherical body of radius >30 km, even if the composition were pure (uncompressed) iron. Any body of that size between the orbits of Atlas and Prometheus should have been discovered by now. Moreover, the observed speed of the pattern, within 1° day^{-1} of the Keplerian rate at the outer edge of the A-ring, is not consistent with the speed of a perturber at the inferred location. It is also not consistent with the speeds of any of the known satellites.

[1] The range in the abscissa in the map projection in Figure 1 corresponds to one orbit at Janus' speed, so anything moving at that rate must appear in the same place, no matter how long the movie is.

7. DISCUSSION

Although the Janus / Epimetheus "swap"—the abrupt change in semimajor axis and the resulting reversal of the satellites' orbital directions in the rotating frame—occurs over a relatively brief period of time (< 1 day), the Cassini imaging data sets obtained 5–8 months before the 2006 January swap show a changing, irregular ring edge that yields a poor fit to the expected $m = 7$ normal mode, as compared to data sets obtained 8 or more months after the swap. Yoder et al. (1983) point out that the angular separation between the satellites, and therefore their respective orbital mean motions (according to Equation (14) of that work), should be changing at their maximum rate as the satellites pass through their Lagrange points at 60° (or ∼ 8 months) separation, so it may be that the resonances are changing location rapidly enough at that time to scramble the ring response. Indeed, Tiscareno et al. (2006) noted a failure in their density-wave model that may have been associated with such an adjustment. Further support for this idea comes from the fact that it took nearly a year to establish the apsidal alignment between the $m = 7$ pattern and Janus after the 2006 January swap.

Nine of the 10 data points fit by Porco et al. (1984) were obtained during the *Voyager 2* flyby in 1981 August, about five months before the 1982 January orbit reversal. Therefore, an adjustment period within ±60° of conjunction probably explains the difference in the $m = 7$ eccentricity and pattern speed between that study and the current one. The smaller eccentricities obtained in the earlier work are comparable to those obtained in this work for observations taken during a comparable phase in libration, i.e., the few months preceding the most recent orbital swap. Moreover, the irregular shape of the pattern, which would not have been evident from the sparse sampling, would have likely corrupted their fit to the pattern speed. The Porco et al. (1984) study also differed from this one in that those data sets were obtained during a time when the co-orbital configuration was opposite to that considered in this work: at that time, the weaker Epimetheus resonance was located inside the ring, while the stronger Janus resonance was outside the ring. Therefore, we expect that the total response would have been smaller in that configuration than in the current one, even if the data had all been obtained farther from the co-orbital swap. Also, since the Epimetheus pattern would have been stronger relative to that of Janus during the *Voyager* epochs, the speed of the net pattern may have been closer to an average, as found in Porco et al. (1984), rather than being dominated by Janus, as observed here. Cassini will continue to observe the rings through the 2010 January swap, so this prediction will soon be tested.

8. CONCLUSIONS

We have examined the outer edge of the A-ring using 24 Cassini imaging data sets consisting of a total of more than 3300 images obtained between days 2005-121 and 2009-036. Our results show that although the A-ring edge is dominated by the expected seven-lobed pattern forced by the 7:6 Lindblad resonance with Janus, there is significant additional structure, which varies significantly with time. Data sets obtained within about eight months (∼ 60°) of the 2006 January conjunction between Janus and Epimetheus show an edge that is irregular compared to those taken at other times, suggesting that a period of adjustment occurs as the satellites approach and recede from each co-orbital swap. That adjustment period may explain the difference in $m = 7$ eccentricity and pattern speed obtained

by Porco et al. (1984) compared to the current work, and is consistent with the observation that the apsidal alignment with Janus was not established until nearly a year after the swap. A substantial periodic variation in the amplitude of the $m = 7$ mode with time corresponds to a beating between the responses raised by the Lindblad resonances with both Janus and Epimetheus, even though the linear theory would predict that Epimetheus' contribution should be negligible. Although short-wavelength undulations suggest the presence of an undetected satellite, no such satellite of the required size exists at the location implied by the simplest possible analysis. These and other radial anomalies seen in some data sets correspond to nothing in classical ring theory, and may arise from the same coupling that could be enhancing the beat pattern.

We acknowledge the staff members within CICLOPS for their dedication and efforts in the design and execution of the ring imaging sequences used in this work. Joe Hahn contributed advice on scientific issues. J.N.S. and C.C.P. were both supported by NASA and the Cassini project. We thank an anonymous reviewer for comments that improved the clarity of the text.

REFERENCES

Acton, C. H. 1990, AIAA and NASA, Intl. Symp. Space Inf. Sys. 2
Antreasian, P. G., et al. 2008, AIAA/AAS Astrodynamics Specialist Conference, AIAA Paper 2008-6747, August 2008
Borderies, N., Goldreich, P., & Tremaine, S. 1982, Nature, 299, 209
French, R. G., et al. 1993, Icarus, 103, 163
Goldreich, P., & Tremaine, S. 1982, Annu. Rev. Astron. Astrophys., 20, 249
Longaretti, P. 1989, Icarus, 82, 281
Porco, C. C. 2005, IAUC, 8524
Porco, C. C., Danielson, G. E., Goldreich, P., Holberg, J. B., & Lane, A. L. 1984, Icarus, 60, 17
Porco, C. C., & Goldreich, P. 1987, AJ, 93, 724
Porco, C. C., et al. 2004, Space Sci. Rev., 115, 363
Porco, C. C., et al. 2005, Science, 307, 1226
Press, W. H., Teukolsky, S. A., Vetterling, W. T., & Flannery, B. P. 1992, Numerical Recipes in C (2nd ed.; New York: Cambridge Univ. Press)
Shu, F. H.. 1984, in Planetary Rings, ed. R. Greenberg & A. Brahic (Tucson, AZ: Univ. Arizona Press)
Spitale, J. N., Jacobson, R. A., Porco, C. C., & Owen, W. M., Jr. 2006, AJ, 132, 692
Tiscareno, M. S., Nicholson, P. D., Burns, J. A., Hedman, M. M., & Porco, C. C. 2006, ApJ, 651, L65
Weiss, J. W., Porco, C. C., & Tiscareno, M. S. 2009, AJ, 138, 272
Yoder, C. F., Colombo, G., Synnott, S. P., & Yoder, K. A. 1983, Icarus, 53, 431